TOWARDS A BETTER UNDERSTANDING OF MULTIPHASE FLOW IN POROUS MEDIA: 3D IN-SITU FLUID DISTRIBUTION IMAGING AT THE PORE SCALE

S. Youssef; D. Bauer; S. Bekri; E. Rosenberg; O. Vizika
IFP, 1 et 4, avenue de Bois-Préau, 92852 Rueil-Malmaison Cedex, France

This paper was prepared for presentation at the International Symposium of the Society of Core Analysts held in Noordwijk, The Netherlands 27-30 September, 2009

ABSTRACT

In this paper we present a new experimental setup combining laboratory high resolution computed micro-tomography (MCT) with a flow microcell specially designed to reproduce in-situ multiphase flow experiments and monitor the fluid distribution at the pore scale. The objective is to describe the fluid saturations and distribution at different steps of the capillary pressure cycle (drainage and imbibition) while maintaining the sample under pressure in the cell to avoid fluid re-distribution. Experiments have been performed on monomodal sandstone where the total porosity is resolved by the MCT. We compared successfully the saturation profiles calculated from the mean grey level of the 2D cross sections and the saturation profiles calculated by 3-phase image segmentation. The two above mentioned methods can be combined in bimodal pore systems to evaluate the fluid saturations in both micro (unresolved) and macro (resolved) porosity. Finally, we describe the distribution of each fluid at the different steps of the cycle and the influence of the pore geometry and interfacial tension on the oil trapping.

INTRODUCTION

Predicting the detailed behaviour of multiphase flow in porous media still presents a challenging domain of increasing interest. Through the past years, many models of fluid displacement mechanisms including fluid/fluid and fluid/solid interface description have been proposed and integrated in numerical modelling schemes like pore network models. The validation of such models is usually done either at the macroscopic level (Bakke et al., 1997, Knackstedt et al., 2004, Laroche et al., 2005) or at the microscopic level using 2D glass micromodels (Lenormand et al., 1988). Detailed experimental data on the 3D flow behaviour at the microlevel have been studied in very few works. Among the pioneers Swanson (Swanson, 1979) combined SEM, Wood's metal porosimetry and acidization to study the distribution of the nonwetting liquid in a variety of porous systems. In a same type of approach (Chatzis et al., 1983) polymerised the nonwetting phase and then studied the structure of residual blobs by SEM.

With the advances of synchrotron MCT over the 3 past decades and more recently the maturity of the laboratory MCT equipments it is now more common to get 3D images of porous media. Since the late 1990s, the introduction of X-Ray absorbent dopants to provide contrast between fluids has enabled non-destructive MCT studies of the 3D distribution of fluids in porous media (Coles et al., 1998). Different systems with different saturation process were imaged. In (Coles et al., 1998, Seright, 2001) a rock is imaged at residual saturation. In (Prodanovic et al., 2006) a specific core holder adapted to synchrotron setup was used and images were taken at different sequences of drainage

and imbibition by injecting for each sequence a constant volume (Vp) of wetting or nonwetting fluid. Turner and co-workers (Turner et al., 2004) drained oil by air gravity and imaged the final state by a laboratory MCT. In another approach (Kumar et al., 2008) the saturation of the porous media was achieved by centrifugation and imaged at the equilibrium state. All these studies give valuable descriptions of the fluid patterns. Nevertheless it is clear that controlling the equilibrium state is one of the difficulties in imaging intermediate saturation states.

The objective of the present paper is to describe at the pore scale the fluid distribution, the fluid/fluid and fluid/solid interfaces as well as their evolution at different steps of the experiment corresponding to different points on the capillary pressure curve (drainage and imbibition). The experiments were realised without any flow interruption which could result in the rearrangement of fluids. A new experimental setup is presented combining laboratory high resolution MCT with a flow cell specifically developed to perform in-situ multiphase flow experiments and to reproduce the classical Hassler type coreholders. Then the different image treatment processes used to extract the quantitative informations from the 3D images are described. Finally some preliminary observations and results on the two phase flow mechanisms are discussed.

Material and Experiment

Hassler microcell

A coreholder was specially designed to allow 3D image acquisition with a pixel size of 5 μm and an in-situ MCT monitoring of the fluid saturations during the experiment. Two conditions were then required: the use of a material transparent to X-rays (PEEK) and the limitation of the size of the cell diameter (10mm). This mini coreholder was designed to reproduce the classical Hassler type coreholders. Three capillary inlets (or outlets) were designed at each side of the cell. One of them was dedicated to the confining pressure, the two others to the arrival (or outlets) of fluids. All the tubes were chosen in order to allow the 360° rotation of the sample during the acquisition and dimensioned to minimize the pressure gradient inside the circuit. A radiograph of the cell showing the two fluid entrances and outlets saturated with oil is shown on **FIG. 1**. This kind of radiographs acquired within a few seconds enables a very easy control of the fluid flow during the experiment.

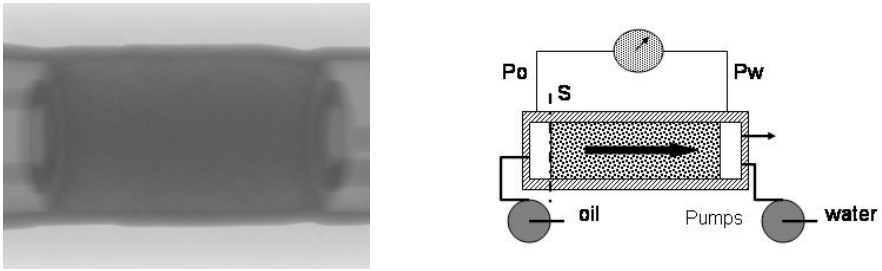

FIG. 1 : Radiograph and schematic representation of the microcell

Sample and fluids

A miniplug was cored in a strongly water-wet Fontainebleau sandstone with 22% mean porosity. The dimension of the miniplug was 6mm in diameter and 7 mm in length. The fluids have been chosen in order to have a good X-Ray absorption contrast. The non wetting phase was a dodecane doped with 25% volume of iododecane and the wetting

phase was pure water. The viscosity ratio of the two fluids is about 1 and the measured interfacial tension was 16.4 mN/m. With these conditions the capillary number varies roughly from 10^{-7} to 10^{-5} depending on the applied flow rate. The Bond number is of the order of 10^{-6}. These values for the Ca and the Bo numbers indicate that capillary forces are the dominant forces against viscosity and gravity.

Permeability measurement

The miniplug sample was loaded into the specially designed mini coreholder and saturated 100% with water. The differential pressure between inlet and outlet pressure of the porous medium has been measured for several water flow rates. Associated pressure gradients are very low, typically a few millibars. A good linearity is observed between the fluid rates and the measured pressure drop. The measured permeability is 2.6D which is in good agreement with the macroscopic measurements.

Fluid flow experiment

In a first step, the plug sample was saturated at 100% with water and imaged to get the first reference scan. For all scan, 1800 radiographs were acquired during the complete 360° rotation of the sample for a total acquisition time of 80min. At this step, a permeability measurement was also performed.

Then, the displacements performed at room conditions, describe a complete capillary pressure cycle: primary drainage, positive spontaneous imbibition (Pc>0), spontaneous imbibition at Pc=0 and forced imbibition. Tagged laboratory oil, containing 25% volume Iododecane as the X-ray blocker, was then injected at different flow rates (0.01, 0.02, 0.04, 0.2 cc/min) to allow the oil saturation within the sample to increase. Water was sweeping at the outlet of the sample in order to maintain the capillary continuity. For more detail on the semi-dynamic method see (Lenormand et al., 1993). The differential pressure measured between the inlet and the outlet of the porous medium was used as a direct measurement of the Pc capillary pressure. Each saturation state was imaged by microtomography with the same parameters as the first reference scan. Injection continued at each rate until equilibrium within the core plug was established, based on the consistency of the saturation profile and differential pressure.

At the end of the drainage cycle, the oil rates were first decreased at the same values as the drainage steps (positive spontaneous imbibition). Then the oil rate was stopped to allow a spontaneous imbibition. MCT acquisitions were done at the very first moments of the spontaneous imbibition and after 3 days. Finally, a water flow rate was imposed (forced imbibition). Effective permeability to water at residual oil saturation was determined after the forced imbibition step. At the end of the cycle miscible displacements were applied in order to saturate the medium with 100% oil and acquire the oil reference images.

3D images of the fluid distribution have been reconstructed for each drainage and imbibition steps at half resolution (10µm) to get the whole sample in one image (750x750x700 voxels). Sub volumes (830x830x1400 voxels) with full resolution (5 µm) were also reconstructed for more detailed quantitative analyses. All the images are coded in 8bits in a normalized grey level. **FIG. 2** shows the grey level histograms of the raw 3D images reconstructed at each step ("step images") of the drainage/imbibition cycle. The water and oil peaks are respectively located on the left side and right side of the matrix (grain) grey level. Selected 2D images are presented in **FIG. 3**: drainage steps for the first line, imbibition steps for the second line. On these images, oil appears in

white and water appears in black. Most of the pores are invaded by the non wetting phase at the third step of the drainage cycle (0.04 cc/min) while most of the pores are invaded by the wetting phase during the first minutes of the spontaneous free imbibition step (Pc=0).

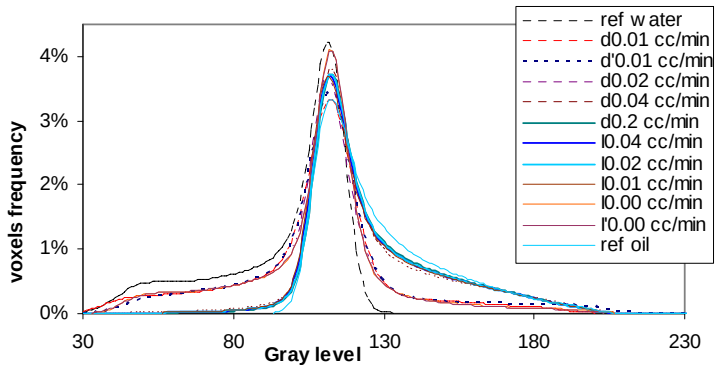

FIG. 2: Grey level histograms of the raw 3D images reconstructed at each step

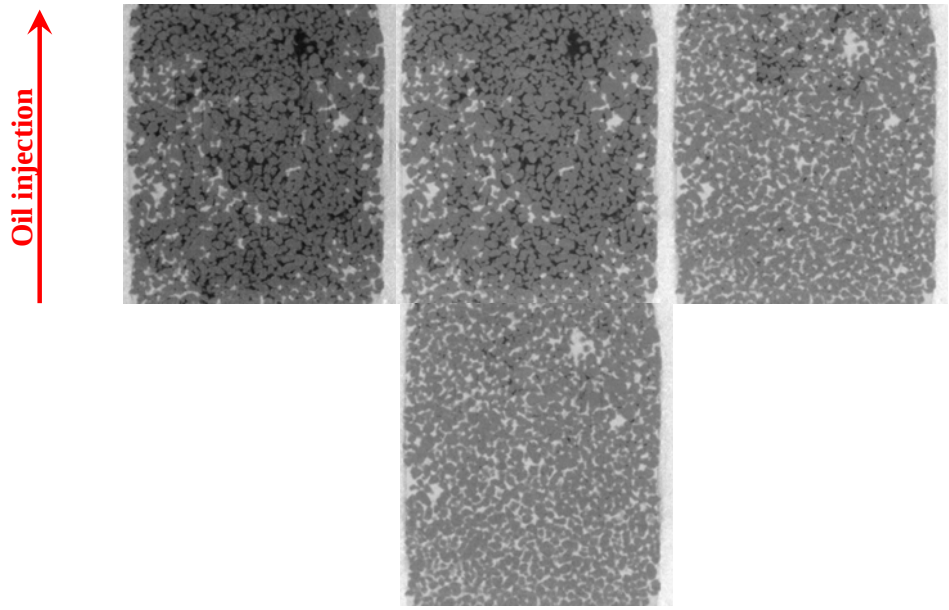

Drainage (0.01cc/min) Drainage (0.02cc/min) Drainage (0.04cc/min) Drainage (0.2cc/min)

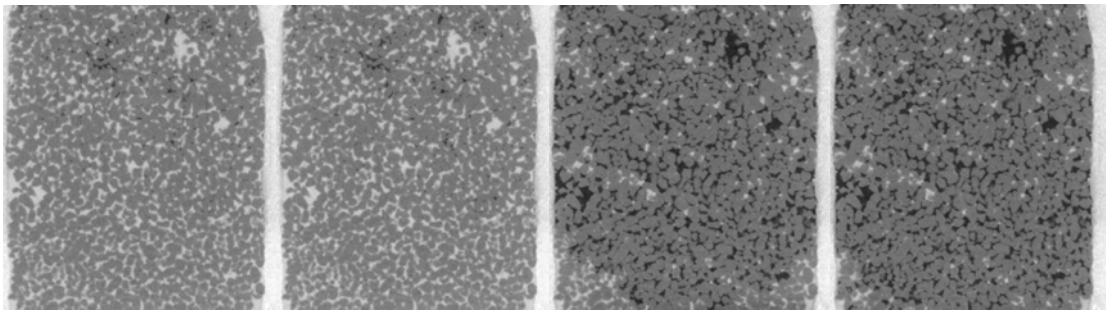

Pc>0 imbibition (0.04cc/min) Pc>0 imbibition (0.01cc/min) Pc=0 FreeSpontaneous imbibition Forced imbibition

FIG. 3: Selected 2D images of the drainage/imbibition experiments

Image treatment

Image registration

Before performing image calculations, registrations have to be done. The reference image was the rock 100% saturated with water. We used the registration module from the commercial code (Avizo^{TM}). The variations between the 100% water saturated image and the step images were less than 0,5° in rotation (mainly in the z-axis) and less than 1 voxel in translation.

Saturation Profiles calculated from the reference images

Saturations were firstly determined slice by slice by the X-ray attenuation method classically used in CT scan studies. For each slice, the mean grey level was measured in the ROI corresponding to the rock cross section and compared to the mean value measured in the same ROI on the reference images. The saturation in the slice was then calculated using the formula:

$$So = \frac{greylevel\ \ (step\ \ \ image) - greylevel\ \ (reference 100\% water)}{greylevel\ \ (reference 100\% oil) - greylevel\ \ (reference 100\% water)}$$

3-phase segmentation

Saturations have also been calculated from the segmented images. This second calculation does not need reference images as in the first case but requires a good contrast between oil and water. The addition of iododecane to the dodecane improves the X-ray attenuation contrast between the oil phase and water. However due to phase contrast, the interfacial area between oil and water appears in the same grey level as the rock phase. The precise location of the solid phase in each image is therefore determined from the reference water saturated image. As the pore space is well resolved we used a simple threshold technique to determine the interface between solid and water phases. In the resulting binary image the solid phase label is 255 and the void space 0. The binary image is then added to each "step image". **FIG. 4** shows the resulting grey level image of the water and oil phase in the same pore. The two phases are well separated as shown in the corresponding histogram and the two fluid contributions can be easily isolated and measured by a simple threshold process.

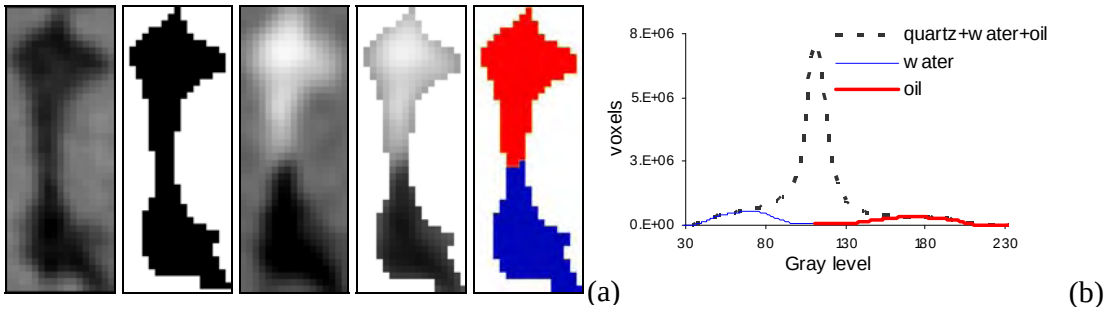

FIG. 4: (a) The different steps of image treatment illustrated on two contiguous pores (b) the grey level contributions of oil and water isolated after the treatment.

The comparison of the results is presented on **FIG. 5**. Dots represent the slice by slice calculation while the lines represent the calculation based on the segmented images. A good agreement is observed between the two ways of calculation. At Swi saturation, water films are not taken into account by segmentation while they are accounted for in the other calculation mode.

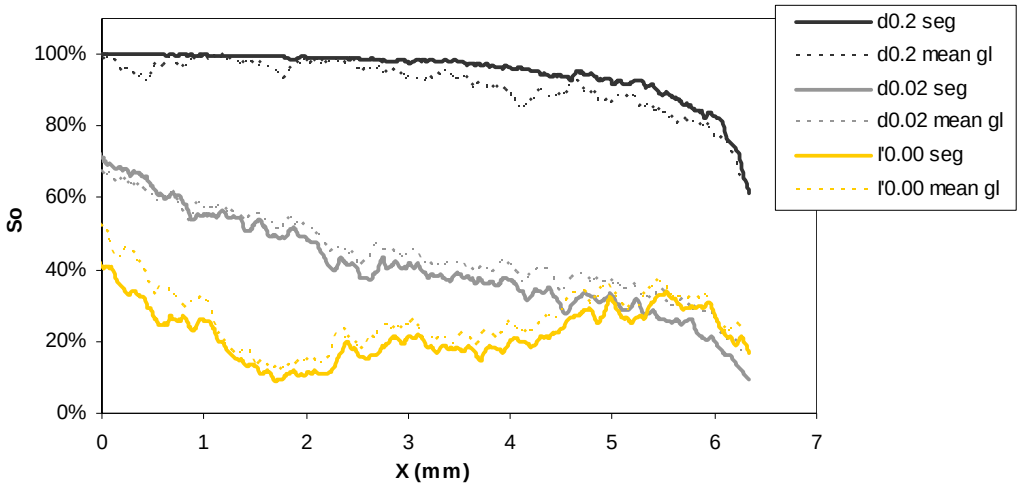

FIG. 5: Comparison of the profiles calculated from the mean grey level (dots) and the profiles calculated by segmentation (lines)

RESULTS AND DISCUSSION

Mean saturations and Pc curve calculation

The oil flow rates, the differential pressure measured during the experiment and the mean saturations measured from the 3D images with the two discussed methods (from references or by segmentation) are presented in Table 1. The entry saturations have also been calculated and used for the Pc curve calculation (red and blue dots in FIG. 6). The experimental drainage Pc=f(So) curve is compared to the drainage Pc curve deduced from a mercury intrusion curve measured on a sister plug. A good agreement is obtained. The imbibition curve is abrupt and most of pore space is saturated with water at Pc=0.

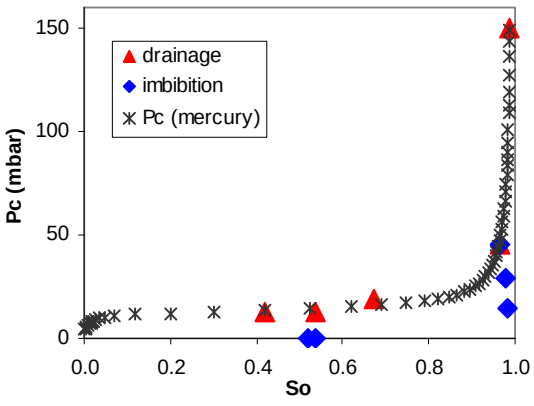

FIG. 6: Experimental Pc curves

image step	flow rate (cc/min)	Pc (mbar)	mean So gl	mean So seg	entry So
d0.01	0.01	13	0.28	0.34	0.42
d'0.01	0.01	13	0.4	0.37	0.54
d0.02	0.02	19	0.48	0.44	0.67
d0.04	0.04	45	0.89	0.92	0.96
d0.2	0.2	150	0.93	0.96	0.99
I0.04	0.04	45	0.91	0.95	0.96
I0.02	0.02	29	0.91	0.95	0.98
I0.01	0.01	15	0.91	0.95	0.98
I0.00	0	0	0.32	0.26	0.54
I'0.00	0	0	0.3	0.26	0.52

Table 1: Mean and entry saturations calculated at each step of the Pc cycle

Drainage cycle

Four different oil flow rates have been applied in the entrance of the sample (0.01, 0.02, 0.04, 0.2 cc/min), while the pressure in the water phase sweeping the outlet of the sample was maintained constant at the atmospheric pressure. The oil saturation profiles at equilibrium for all four flow rates are given in **FIG. 7.** For comparison purposes an

intermediate profile for the lowest flow rate is also presented in the same figure. At each flow rate the oil enters progressively in the porous medium until equilibrium is reached. The profiles are typical of drainage process at low capillary number. The form of the profiles indicates that there has been no sharp displacement front. This is also confirmed on the 3D distributions of the fluids shown in **FIG. 7**. Images are characteristic of a low capillary number drainage ($Ca \sim 10^{-6}$). Indeed it is evidenced that severe microfingering occurred mostly along the walls leading to an early breakthrough of the invading phase (oil). Then at each increasing flow rate the microfingers expand laterally displacing more and more water and filling the space almost exclusively with oil. The saturation profiles show that for the highest flow rate the water saturation (yellow colour in the last image) is very low throughout the sample and most of this water is accumulated in the outlet, in agreement with a classical capillary retention of the wetting phase drained by a non-wetting phase. Most of the porosity is drained between the 2 steps 0.02 and 0.04cc/min which correspond to the plateau of the capillary pressure curve (cf. **FIG. 6**).

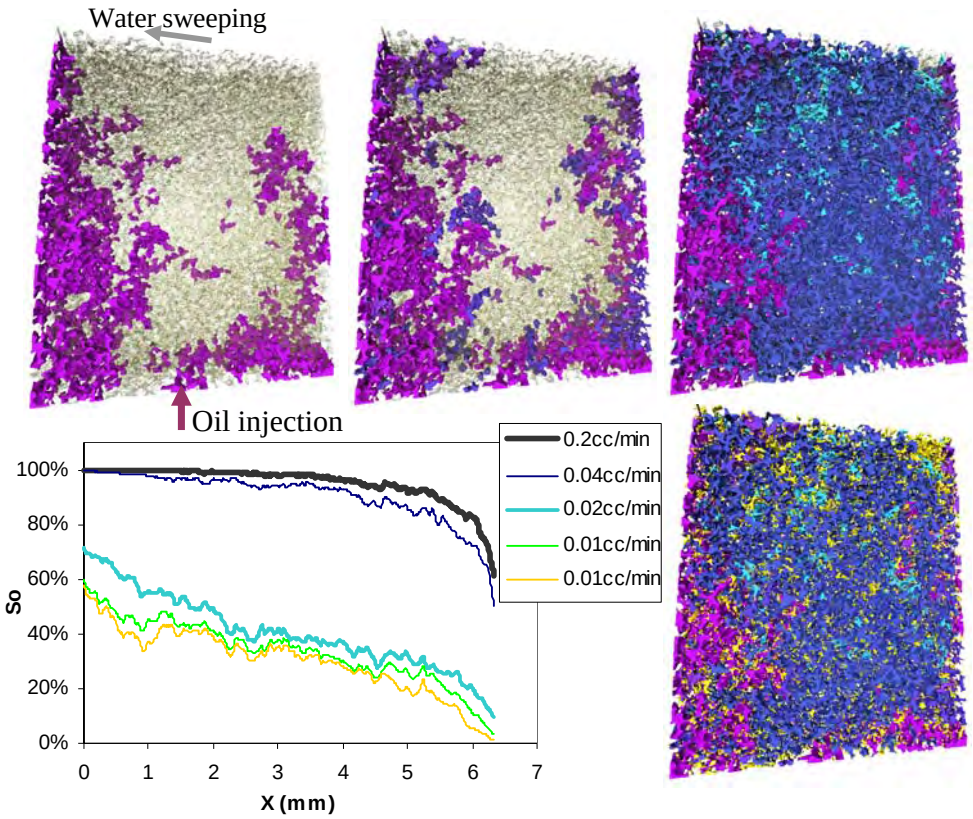

FIG. 7: 3D distribution of fluids during the drainage cycle (purple d0.01, dark blue d0.02, blue d0.04 and light blue d0.2, yellow=Swi) and corresponding saturation profiles

Imbibition cycle

The imbibition cycle started with the fluid distribution attained in the last stage of the drainage cycle (S_{wi}, with a capillary retention in the outlet). The oil flow rate was progressively decreased following the same rate values as those selected during the drainage process while maintaining at the outlet the previous water phase sweeping. For very small changes of the flow rate, the conditions are those of a quasistatic spontaneous imbibition. At the beginning the displaced phase (oil: receding phase) is completely connected and the water-oil interfaces reside in the entrance of the pores near the

sample inlet. The capillary suction is strongest in the smallest pores. The displacement advances through a succession of capillary displacements, each time in the narrowest available pore. Once a pore is invaded, all the adjoining throats are invaded. The quasistatic spontaneous imbibition (Pc>0) does not seem to affect the mean saturation (**FIG. 8**). Very low local changes of saturation are observed on the local saturation images (**FIG. 9**) even after 24h per step and 3 steps (blue points cumulate water volume of the 3 steps) which suggests a sharp spontaneous imbibition Pc curve. The fact, however, that changes of the saturation, even slight, are observed very far from the main water/oil front indicates the role of the wetting films and wetting phase pendular structures in its advancement and the corresponding trapping of the oil. This is also relevant to the capillary hyperdiffusion phenomenon first observed experimentally in porous media by (Bacri et al., 1985).

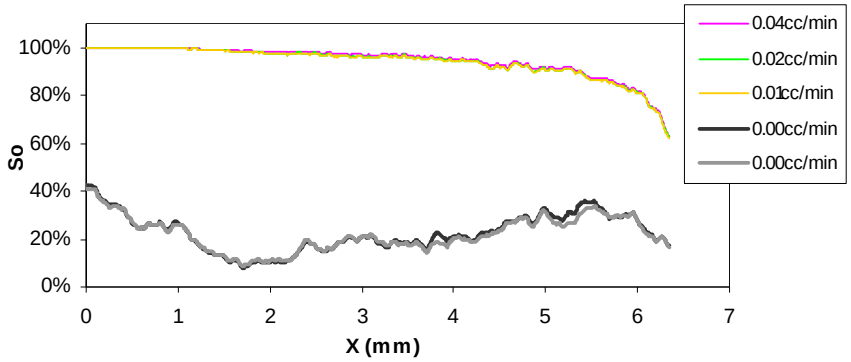

FIG. 8 : Saturation profiles of the imbibition cycle

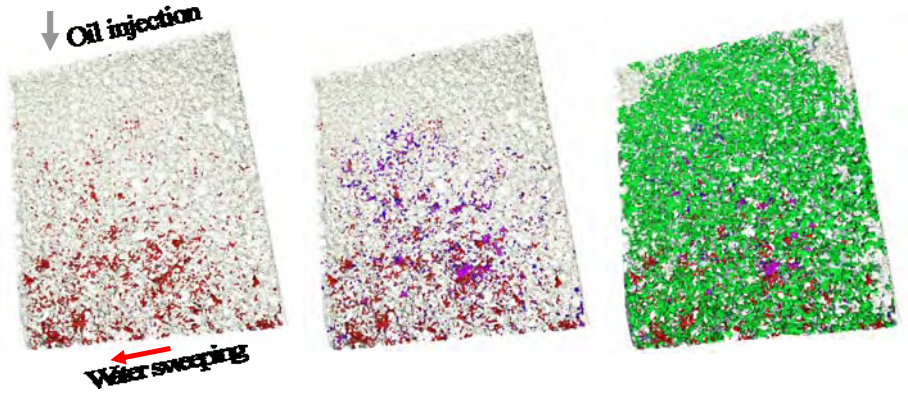

FIG. 9: 3D distribution of fluids during the imbibition cycle (Swi, spontaneous imbibition at Pc>0, and free spontaneous imbibition at Pc=0)

The quasistatic spontaneous imbibition (Pc>0) is followed by a spontaneous imbibition step at Pc=0. This results in an instantaneous and complete invasion of the pore volume by water, green coloured (large plateau of the saturation for Pc =0). Indeed this spontaneous imbibition experiment at Pc=0 is the equivalent of a free imbibition test. Contrary to controlled Pc>0 quasistatic imbibition, free imbibition advances in many pores simultaneously. Due to this parallel rather than sequential mode of invasion the displacement patterns are not the same as for quasistatic imbibition. But the most important difference between quasistatic and free imbibition is in terms of the capillary number. While in the quasistatic conditions Ca is very low, in free imbibition conditions relatively large Ca values can be obtained globally and locally depending on the pore

geometry, the length of the medium and the properties of the fluids (Payatakes et al., 1984). As a result a good sweeping of the non-wetting phase can be obtained, while its saturation may locally go down to less than 0.1 (**FIG. 8**).

FIG. 10 shows the microscopic distribution of the oil trapped phase after the free spontaneous imbibition step. It is seen that the non-wetting phase is trapped in a multitude of small ganglia of sizes going from smaller than one to several pores. These ganglia are more or less uniformly distributed within the pore space (bottom left image). Some characteristic detailed views are also given in the same figure. Even though it is difficult to analyse the stability of each ganglion without a detailed knowledge of the local geometrical and topological characteristics and of their orientation compared to the local flow direction, it is easier to understand that mobilisation of this trapped phase is impossible without an important change of the capillary conditions (i.e. flushing with a fluid of very low interfacial tension).

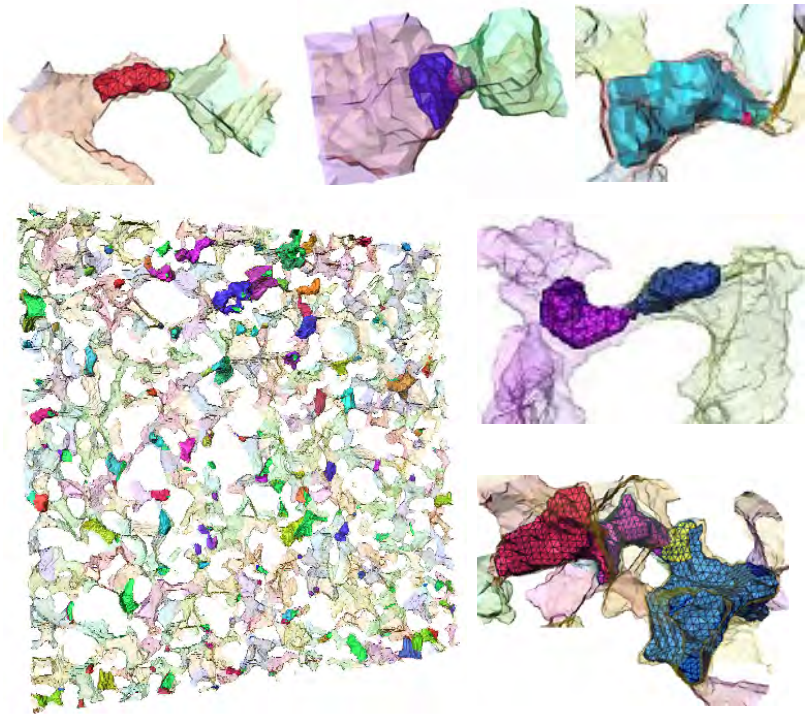

FIG. 10: 3D view of a subvolume at residual oil saturation) – Detailed views of different trapped oil blobs configurations (throat, blob squeeze, single pore body, doublet around a throat, cluster)

Effect of interfacial tension

In order to study the effect of interfacial tension on the trapping of oil, a new drainage/imbibition cycle has been performed with a second set of fluids on the same miniplug. Oil was pure dodecane while brine was a 60g/l of potassium iodide solution; the interfacial tension was 40 mN/m instead of 16 mN/m. At the end of the cycle, the trapping configurations have been compared to the previous one. **FIG. 11** shows the same 3D area and the same zoomed area for the high interfacial tension experiment (purple colour) and the low interfacial tension experiment (red colour). Most of the oil seems to be trapped in the same areas of the 3D pore network. However, some of the oil blobs are more connected to each other therefore occupying several adjacent pore bodies in the second experiment (high interfacial tension).

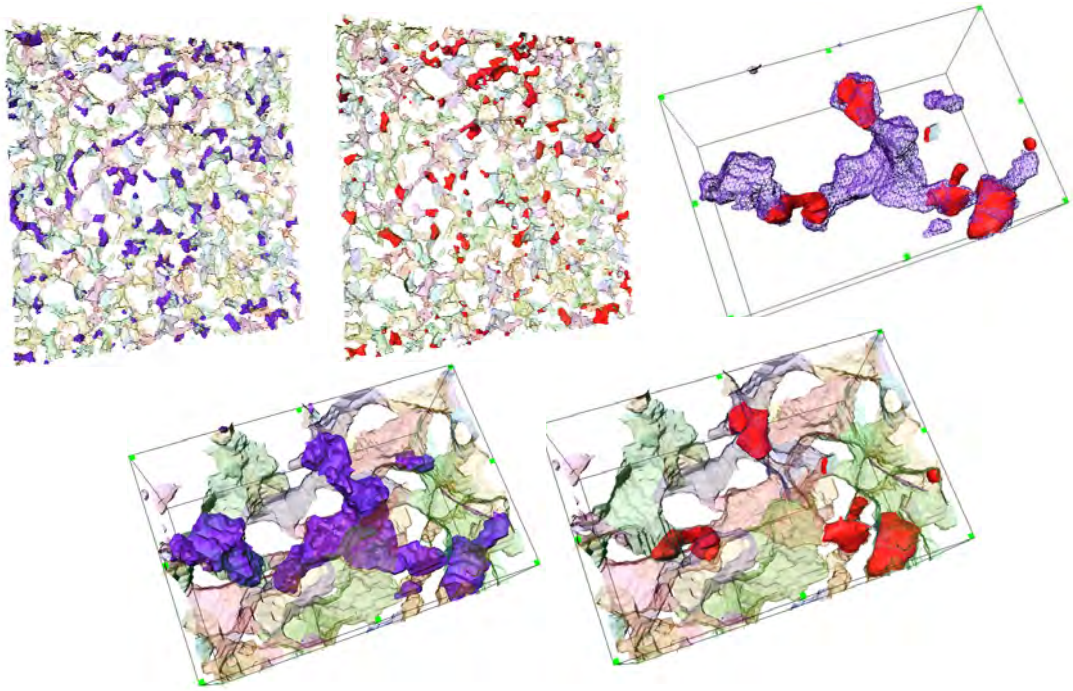

FIG. 11 : Comparison of residual oil saturation and trapping configurations for two interfacial tension values after imbibition on the same rock sample (purple γ_{ow}=40 mN/m, red γ_{ow}: 16 mN/m). Zoomed view showing the two oil trapping configurations and separate views of the oil ganglia.

Drainage and imbibition comparison at identical saturation

In **FIG. 12** a comparison is made of the oil distribution for drainage versus imbibition conditions within the same sub volume at a same saturation level (So=23%). It is seen that under drainage conditions oil is continuous, forming a network occupying the biggest pores, and advancing through compact displacement mechanism. For imbibition conditions the same quantity of oil is discontinuous and very dispersed, still occupying the big pores but forming isolated ganglia. The water/oil interface in imbibtion conditions is 1.5 times higher than in drainage conditions. This difference can explain the hysteresis observed in the non-wetting phase relative permeability curves under strong wettability conditions as well as in the Pc curve (Joekar-Niasar et al., 2008).

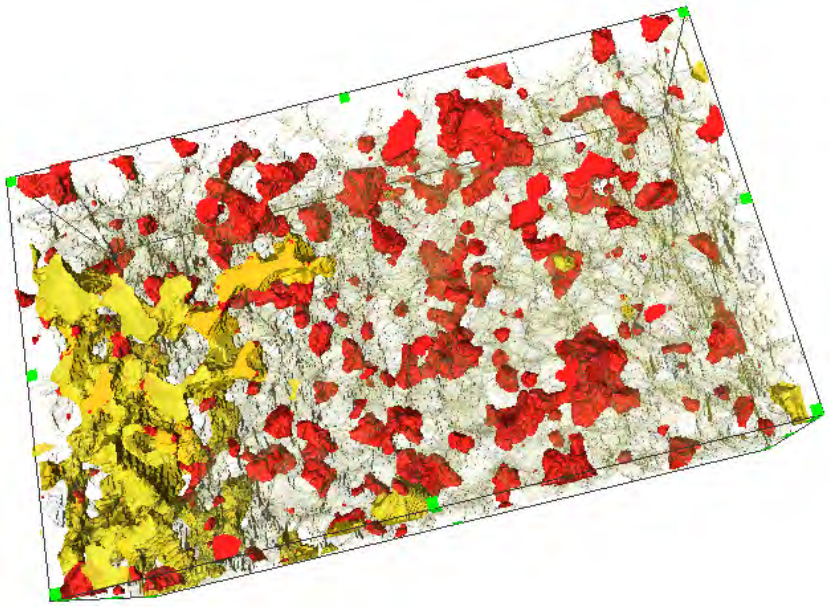

FIG. 12: Comparison of the oil distribution in the same subvolume at identical saturations (red= imbibition, yellow=drainage)- The surface area developed by oil is 1.5 larger in the imbibition image

CONCLUSION

In this paper we present a new laboratory MCT in-situ setup enabling 3D observation of multiphase fluid distribution in porous media under continuous flow conditions. The experimental set-up that combines a laboratory X-ray microtomograph and a specially designed flow cell was tested and validated on a sandstone sample. A set of image processing tools were used and methodologies developed to access the spatial distribution of the different fluid (oil / water) in the pore space. The qualitative observation of the residual oil saturation shows different trapping configurations of oil blobs which are not necessary in the centre of the biggest pores. Preliminary results on the effect of interfacial tension on the trapping configuration show local differences on the blobs connectivity and local saturation. Finally we compared the developed water/oil interfaces in imbibition and drainage conditions within a subvolume at equal saturation and found a significant difference that can explain the hysteresis observed on the Kr and Pc curves. This development will help in studying multiphase displacements in 3D complex networks and the impact of flow conditions and fluid properties. The set of 3D images following step by step the drainage/imbibition cycle in a model rock constitutes a useful data base for testing the mechanisms used in the PNM codes for the simulation of petrophysical properties.

ACKNOWLEDGMENTS

We would like to thank Herve Deschamps and Marianna Rondon Gonzalez for there valuable assistance in the experiment.

REFERENCES

1. Bacri, J.C., C. Leygnac, and D. Salin: "Evidence of Capillary Hyperdiffusion in 2-Phase Fluid-Flows," *Journal de Physique Lettres* (1985), 46, 467-473.
2. Bakke, S. and P.E. Oren: "3-D Pore-Scale Modelling of Sandstones and Flow Simulations in the Pore Networks," *Spe Journal* (1997), 2, 136-149.
3. Chatzis, I., N.R. Morrow, and H.T. Lim: "Magnitude and Detailed Structure of Residual Oil Saturation
44," *Society of Petroleum Engineers Journal* (1983), 23, 311-326.
4. Coles, M.E., R.D. Hazlett, E.L. Muegge, K.W. Jones, B. Andrews, B. Dowd, P. Siddons, A. Peskin, P. Spanne, and W. Soll: "Developments in synchrotron X-ray microtomography with applications to flow in porous media," *Spe Reservoir Evaluation & Engineering* (1998), 1, 288-296.
5. Joekar-Niasar, V., S.M. Hassanizadeh, and A. Leijnse: "Insights into the relationships among capillary pressure, saturation, interfacial area and relative permeability using pore-network modeling," *Transport in Porous Media* (2008), 74, 201-219.
6. Knackstedt, M.A., C.H. Arns, A. Limaye, C.H. Arns, A. Limaye, A. Sakellariou, T.J. Senden, A.P. Sheppard, R.M. Sok, W.V. Pinczewski, and G.F. Bunn: "Digital core laboratory: Reservoir-core properties derived from 3D images," *Journal of Petroleum Technology* (2004), 56, 66-68.
7. Kumar, M. et al.: "Imaging of core scale distribution of fluids and wettability", *Int. Sym. of the Society of Core Analysts*, Abu Dhabi, UAE (2008) .
8. Laroche, C. and O. Vizika: "Two-phase flow properties prediction from small-scale data using pore-network modeling," *Transport in Porous Media* (2005), 61, 77-91.
9. Lenormand, R., A. Eisenzimmer, and C. Zarcone: "A novel method for the determination of water/oil capillary pressures of mixed wettability samples", *Int. Sym. of the Society of Core Analysts*, Houston, Texas (1993) .
10. Lenormand, R., E. Touboul, and C. Zarcone: "Numerical models and experiments on immiscible displacements in porous media," *J Fluid Mech* (1988), 198, 165-187.
11. Payatakes, A.C. and M.M. Dias: "Immiscible Microdisplacement and Ganglion Dynamics in Porous Media," *Reviews in Chemical Engineering* (1984)174
12. Prodanovic, M., W.B. Lindquist, and R.S. Seright: "Porous structure and fluid partitioning in polyethylene cores from 3D X-ray microtomographic imaging," *Journal of Colloid and Interface Science* (1-6-2006), 298, 282-297.
13. Seright, R.S.: "Gel propagation through fractures," *Spe Production & Facilities* (2001), 16, 225-231.
14. Swanson, B.F.: "Visualizing Pores and Non-Wetting Phase in Porous Rock 179," *Journal of Petroleum Technology* (1979), 31, 10-18.
15. Turner, M.L., L. Knufing, C.H. Arns, A. Sakellariou, T.J. Senden, A.P. Sheppard, R.M. Sok, A. Limaye, W.V. Pinczewski, and M.A. Knackstedt: "Three-dimensional imaging of multiphase flow in porous media," *Physica A-Statistical Mechanics and Its Applications* (1-8-2004), 339, 166-172.